

Shining X-rays on asymptotically safe quantum gravity

Biao Zhou,¹ Askar B. Abdikamalov,¹ Dmitry Ayzenberg,^{1,2}
Cosimo Bambi,^{1,*} Sourabh Nampalliwar,² and Ashutosh Tripathi¹

¹*Center for Field Theory and Particle Physics and Department of Physics, Fudan University, 200438 Shanghai, China*

²*Theoretical Astrophysics, Eberhard-Karls Universität Tübingen, 72076 Tübingen, Germany*

Asymptotically safe quantum gravity is a promising candidate scenario to provide a UV extension for the effective quantum field theory of Einstein's gravity. The theory has its foundations on the very successful framework of quantum field theory, which has been extensively tested for electromagnetic and nuclear interactions. However, observational tests of asymptotically safe quantum gravity are more challenging. Recently, a rotating black hole metric inspired by asymptotically safe quantum gravity has been proposed, and this opens the possibility of astrophysical tests of the theory. In the present paper, we show the capabilities of X-ray reflection spectroscopy to constrain the inverse dimensionless fixed-point value γ from the analysis of a *Suzaku* observation of the X-ray binary GRS 1915+105. We compare these constraints with those obtained from black hole imaging.

I. INTRODUCTION

Einstein's theory of gravity, known as general relativity, is the standard theory to describe gravitational phenomena in our Universe. Since it was proposed back in 1915, a large variety of experiments have been performed to check its veracity. For most of history, these tests were able to probe only the weak-field regime [1], and general relativity (GR hereafter) proved to be highly successful. The story in the strong-field regime is quite interesting. Over the past few years, tests in the strong-field regime have become commonplace [2–5]. While largely successful here too, some features of GR in the strong-field regime render it unsuitable as the final theory. These include the presence of singularities, and the difficulties to find a theory of quantum gravity beyond an effective low-energy model. Both these issues suggest that there is some theory that supersedes GR, and of which GR is the low energy limit. Various proposals of such superseding theories are matters of active research, the most popular ones being string theory and loop quantum gravity. For any such proposal, determining its veracity is impossible if its predictions are not testable.

Naïvely merging GR with quantum mechanics results in a failure, due to the unfortunate fact that GR is non-renormalizable. Workarounds have been found to resolve this issue, one of them being the idea of asymptotic safety. The basic idea of asymptotically safe gravity is the following: quantum fluctuations modify the standard gravitational interactions by making them scale dependent. This can be achieved by turning the Newton's coupling constant G_N into a length dependent constant $G_N(r)$. But such a modification can result in infinities in the theory, which is a deal-breaker. In typical quantum field gravity, this problem is resolved by invoking asymptotic freedom, which prescribes that particle interactions become asymptotically weaker as the corresponding length scale decreases. But in GR modified

with a scale dependent $G(r)$, perturbative renormalization breaks down, rendering asymptotic freedom impossible. The resolution lies in asymptotically safe gravity. In such a setting, the dimensionless coupling parameter ($g(k) \equiv G_N(k) k^2$, where k is the Renormalization Group energy scale) becomes constant below a certain length scale. The above condition can be reformulated as [6]

$$G_N(k) = \frac{g_*}{k^2}, \quad (1)$$

where g_* is the asymptotically safe fixed-point value. This results in an effective weakening of gravity above certain energy scales (equivalently, below certain length scales).

Black holes (BHs hereafter) are objects which, owing to their compactness, exhibit strongest gravitational effects in our Universe. Their simple structure within GR implies that any beyond-GR feature, if imprinted on the BH, will be easily identified. Moreover, they are present in large numbers in the Universe. All these features make BHs the best probes of testing gravity in our Universe. Within GR, BHs have at most three free parameters - mass, spin and charge.¹ Astrophysically, charged BHs are not expected to be common [8], thus only two parameters, mass and spin, characterize all astrophysical BHs [9, 10]. In asymptotically safe gravity, BH solutions are modified [6]. Their deviation from GR BH solutions is parameterized by g_* .

Over the past few years, three different approaches for probing the strong gravity effects around BHs have been realized. Gravitational waves, mostly from binary mergers at present but also from extreme mass ratio inspirals in future, are expected to be the best probes of strong gravity, though in some cases, it is expected to be comparable [11] or weaker [12, 13] than other techniques. X-ray spectroscopy is a very promising technique [2, 14, 15] and is quite advanced as compared to some other techniques,

* Corresponding author: bambi@fudan.edu.cn

¹For assumptions that go in arriving at this conclusion, see [7].

but suffers from parameter degeneracies and limited astrophysical modelling. BH imaging is the latest and a quite exciting potential technique for probing the regions very close to the BH, but is not expected to provide very strong constraints on alternative theories [5, 16].

Modified BHs of asymptotically safe gravity have been analyzed with one of these approaches. In [6], the authors analyze the shadows from regular GR BHs and the modified BHs of asymptotically safe gravity. Our aim in the present paper is to add to this program by analyzing these modified BHs with X-ray reflection spectroscopy. The standard model for analyzing X-ray reflection from astrophysical sources assuming GR BHs, RELXILL [17, 18], has been extended to non-GR BHs with the RELXILL_NK suite of models [19, 20]. Various non-GR theories and deviation parameters have been tested with this approach [21–34], and a public version of the model is available at [35, 36]. We have implemented the BH solutions of asymptotically safe gravity in the RELXILL_NK framework. Furthermore, we have used this framework to analyze data from an X-ray binary in our Galaxy to get astrophysical bounds on the g_* parameter.

Since astrophysical BHs mostly are rotating, and X-ray spectroscopy is at its best for rapidly rotating BHs, we shall focus on rotating BH solutions in asymptotically safe gravity. The rest of the paper is organized as follows: in Sec. II, we review the BH solutions in asymptotically safe gravity. A review of X-ray spectroscopy, the RELXILL_NK framework, and the numerical techniques used is provided in Sec. III. Sec. IV details the X-ray source, observation and data analysis. Data analysis results are discussed and a comparison with previous works is presented in Sec. V.

II. THE METRIC

To arrive at BH solutions in asymptotically safe gravity, [6] prescribes two steps. Firstly, the Newton's Coupling constant G_N is replaced with the generalized length dependent $G_N(k)$, to include effects of quantum fluctuations of gravity. Secondly, the Renormalization Group energy scale k is identified with a characteristic scale of the classical spacetime. This gives a modified BH metric. We follow this prescription now, as given in [6], to generalize the Kerr metric. The usual Kerr metric in Boyer-Lindquist coordinates is given as

$$\begin{aligned}
 ds^2 = & -\frac{\Delta_r - a^2 \sin^2 \theta}{\rho^2} dt^2 + \frac{\rho^2}{\Delta_r} dr^2 + \rho^2 d\theta^2 \\
 & + \frac{(a^2 + r^2)^2 - a^2 \Delta_r \sin^2 \theta}{\rho^2} \sin^2 \theta d\phi^2 \\
 & - \frac{2(a^2 + r^2 - \Delta_r)}{\rho^2} a \sin^2 \theta dt d\phi
 \end{aligned} \quad (2)$$

Here, a is the specific angular momentum, defined as $a = J/M$, and

$$\rho^2 = r^2 + a^2 \cos^2 \theta, \quad (3)$$

$$\Delta_r = r^2 + a^2 - 2GM r. \quad (4)$$

The first step is to generalize G to $G_N(k)$, which is given as

$$G_N(k) = \frac{G_0}{1 + \gamma G_0 k^2}. \quad (5)$$

The second step is to identify k with a scale in the spacetime, which is done as follows

$$k^2 = \frac{G_0 M r^3}{\rho^6}. \quad (6)$$

Thus, our modified-Kerr metric has one extra free parameter γ , the inverse dimensionless fixed-point value ($\gamma = g_*^{-1}$).

We will work in the so called natural units. In these units, the gravitational radius is given as

$$r_g = M/M_{\text{Pl}}^2, \quad (7)$$

and

$$G_0 = 1/M_{\text{Pl}}^2, \quad (8)$$

where M is the BH mass parameter, and M_{Pl} is the Planck mass. Finally, we define a scaled γ parameter as follows

$$\tilde{\gamma} = \frac{\gamma M_{\text{Pl}}^2}{M^2}. \quad (9)$$

For the rest of the paper, we will use $\tilde{\gamma}$ as our deformation parameter.

III. X-RAY REFLECTION SPECTROSCOPY

A. Theory

X-ray spectroscopy is based on the fundamental phenomenon of matter accreting on BHs. As matter falls from a companion star (in case of stellar-mass BHs) or galactic material (in case of supermassive BHs) into a BH, it heats up. During the accretion process, various high-energy processes lead to a plethora of radiation being emitted. These photons climb the gravitational well of the BH, traverse the universe and are detected by X-ray telescopes stationed around the Earth. Effects of the interstellar/intergalactic media, the BH neighborhood and the BH itself are imprinted on the observed spectra.

Fig. 1 presents a schematic diagram of the BH neighborhood. The BH is at the center of the system, and in our case is given by Eq. 2. The disk is the standard Novikov-Thorne type disk [37] with the following properties in particular: optically thick, geometrically

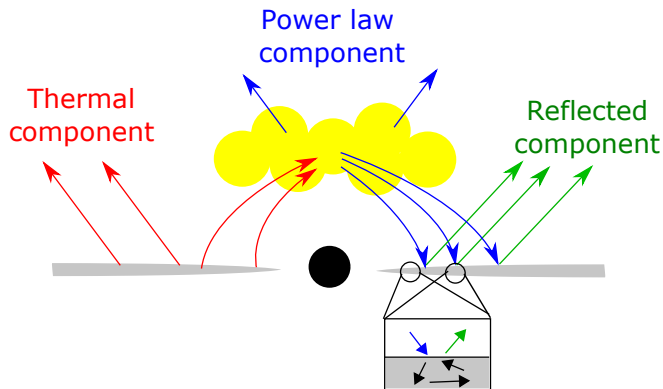


FIG. 1. A schematic diagram of the disk-corona model. The central black circle denotes the BH. The disk is indicated in grey, and the corona in yellow. The coronal morphology is poorly understood so this illustration is only a guess. The arrows indicate photons and are colored according to the classification labeled on the figure and discussed in the text.

thin, equatorial and no magnetic fields. (For all disk properties, see the reference above.) The size of disk is parametrized with r_{in} and r_{out} which quantify the inner and the outer edge of the disk, respectively. Additionally, the system includes a “corona”. It is a source of very high energy photons, with effective temperatures of the order of 100 keV, compared to the disk where effective temperatures are given as [38]

$$T_{\text{eff}} \sim \left(\frac{10}{M}\right)^{1/4} \text{ keV}, \quad (10)$$

where M is the BH mass in the units of solar mass, and are of the order of 1 keV for stellar-mass BHs and 0.01 keV for supermassive BHs. The formation and morphology of the corona is a topic of active research and is probably different for different sources (e.g., it could be the base of an astrophysical jet [39], or a ring of high energy electrons above the accretion disk [40]).

Given the plethora of high-energy processes happening in the BH neighborhood, the observed spectra is mixture of radiation of varied origins. For the model described in Fig. 1, the total spectrum has three components. Firstly, the particles in the disk give off thermal radiation. As particle speeds vary along the disk, the total thermal radiation is given by a multicolor blackbody radiation. Secondly, some of these thermal photons interact with the corona and, as a result of Compton upscattering, contribute a *power-law* component to the total spectrum. Thirdly, those upscattered photons that impinge the disk, get reprocessed and are reflected back, giving rise to a *reflected* component. Among the three, the power-law component is not very informative about the metric, and the thermal component is only weakly informative. The reflected component is most important for our purpose, and we describe now how the asymptotically free metric shown in Eq. 2 was implemented in a reflection model.

B. The RELXILL_NK model

The reflection component is sensitive to not just the BH (which determines particle motion in the disk and the photon trajectory from the point of emission to the telescope) but also to the structure and composition of the disk, as well as the corona. Reflection models therefore must include parameters related to all the aspects of the disk-corona model. To this end, a suite of models, called RELXILL_NK [19, 20, 35, 36], has been developed. It is built for the standard X-ray data analysis software XSPEC and includes a large class of BH-disk-corona models. It can model both the reflection and the power-law components of the spectrum. The eponymous model is described below.

Parameter	Default value
q_{in}	3
q_{out}	3
$r_{\text{br}} [M]$	15
spin	0.998
i [deg]	30
r_{in} [ISCO]	1
$r_{\text{out}} [M]$	400
Γ	2
$\log \xi$	3.1
A_{Fe}	1
E_{cut} [keV]	300
R_f	3
δ -type	1
δ -value	0
N	1

TABLE I. The parameters included in the RELXILL_NK model and their default values. The units of the parameters, where applicable, are indicated. In particular, r_{in} is specified in units of ISCO by default, but can also be specified in units of M .

Tab. I lists the the basic RELXILL_NK model parameters and their default values. These parameters describe different aspects of the system, as follows.

- The spacetime is modeled using three parameters: a_* specifies the BH spin, δ -type is an integer that is used to switch between different deformation parameters, and δ -value specifies the value of the chosen deformation parameter.²

²Note that the BH mass is not a model parameter since, unlike the thermal spectrum, the reflection spectrum does not depend on the BH mass explicitly.

- The emissivity profile of the disk is modeled as a power law as follows:

$$I \propto \frac{1}{r^{q_{\text{in}}}} \quad \text{if } r < r_{\text{br}},$$

$$I \propto \frac{1}{r^{q_{\text{out}}}} \quad \text{if } r \geq r_{\text{br}}.$$

The following assumptions are made about the disk structure: it is assumed to be infinitesimally thin, confined in the equatorial plane and particles in the disk move in quasi-geodesic circular orbits. Thus only two structure parameters are needed to describe the disk structure, viz. r_{in} and r_{out} , the inner and the outer radius of the disk, respectively.

- The composition of the disk is assumed to follow our sun, i.e., the relative elemental abundances follow their solar values. The notable exception is iron, which is modeled with A_{Fe} , defined as the ratio of iron content in the disk and the iron content in the sun. This is to account for higher (or lower) iron content in the accretion disks, as it depends on the history of the constituents that make up the disk. Besides this, $\log \xi$ parametrizes the ionization of the disk (where ξ is in units of erg cm/s), and ranges from 0 (neutral) to 4.7 (highly ionized).
- The coronal emission is taken care of with Γ , which is the index of the power-law component, and the high energy cut-off E_{cut} , beyond which the power-law component is exponentially suppressed. The latter is a feature that can be inferred from observations and must be included if we have data covering the hard X-ray spectrum.
- Since the model includes both the power-law and the reflection component, R_f is provided to control the relative contributions of the two components. It is defined as the ratio of intensity emitted towards the disk and that escaping to infinity.
- The observer's viewing angle is accounted with i and the overall normalization with N .

Other models in the RELXILL_NK suite change one or more aspect of the basic model, e.g., RELXILLP_NK assumes the corona is a point source on the BH spin axis, RELXILLD_NK allows for higher electron density in the disk, and so on. For a complete list of models in the

RELXILL_NK suite, please see [20].

C. Numerical method

We now describe how the metric in Eq. 2 was implemented in the RELXILL_NK model. The output of the model includes the reflection spectrum at the telescope screen. This is given as

$$F_o(\nu_o) = \int I_o(\nu_o, X, Y) d\tilde{\Omega}, \quad (11)$$

Here I_o is the specific intensity (e.g., in units of erg s⁻¹ cm⁻² str⁻¹ Hz⁻¹) as detected at the telescope, X and Y are the Cartesian coordinates of the image of the disk in the screen of the telescope, and $d\tilde{\Omega} = dXdY/D^2$ is the element of the solid angle subtended by the image of the disk in the telescope screen. $d\tilde{\Omega}$ can be recast using the redshift factor and the transfer function [41]. The former is defined in terms of the photon's frequency in the telescope's frame of reference at the point of detection, ν_o , and the same in the emitter's rest frame at the point of emission, ν_e , as follows:

$$g = \frac{\nu_o}{\nu_e}. \quad (12)$$

The latter is defined as follows:

$$f(g^*, r_e, i) = \frac{1}{\pi r_e} g \sqrt{g^*(1-g^*)} \left| \frac{\partial(X, Y)}{\partial(g^*, r_e)} \right|. \quad (13)$$

where r_e is the radial coordinate at the point of emission on the disk and g^* is the normalized redshift factor, defined as

$$g^* = \frac{g - g_{\text{min}}}{g_{\text{max}} - g_{\text{min}}}, \quad (14)$$

where $g_{\text{max}} = g_{\text{max}}(r_e, i)$ and $g_{\text{min}} = g_{\text{min}}(r_e, i)$ are, respectively, the maximum and the minimum values of the redshift factor g at a fixed r_e and for a fixed inclination angle of the telescope relative to the BH spin axis. I_o can be recast using the Liouville's theorem:

$$I_o = g^3 I_e, \quad (15)$$

in terms of the redshift factor and I_e , the specific intensity at the point of emission. This results in the following expression for the flux.

$$F_o(\nu_o) = \frac{1}{D^2} \int_{r_{\text{in}}}^{r_{\text{out}}} \int_0^1 \pi r_e \frac{g^2}{\sqrt{g^*(1-g^*)}} f(g^*, r_e, i) I_e(\nu_e, r_e, \vartheta_e) dg^* dr_e. \quad (16)$$

Here D is the distance of the observer from the source and ϑ_e is the photon's direction relative to the disk at the point of emission. The r_e -integral ranges from the

inner to the outer edge of the disk, and the g^* -integral ranges from 0 to 1.

The introduction of the transfer function enables a sep-

aration between the microphysics at the disk and the photon travel along the null geodesic. The reflection spectrum can be readily calculated using Eq. 16 if the transfer function is known. But the high computational cost to calculate the transfer function by tracing photons and using Eq. 13 whenever the flux needs to be calculated, prohibits the direct usage these equations. Rather, the RELXILL_NK framework uses interpolation schemes to calculate the transfer function for any $\{g^*, r_e, i\}$ from the transfer functions for some $\{g^*, r_e, i\}$. The transfer function data for some $\{g^*, r_e, i\}$ is stored in a FITS (Flexible Image Transport System) table. The procedure to create such a table is described in [19, 20]. We briefly overview this scheme here.

The three model parameters spin a_* , deformation parameter $\tilde{\gamma}$ and the telescope’s inclination angle i , are discretized in a $36 \times 30 \times 22$ grid, respectively. The grid spacing in each dimension is non-uniform, e.g., the grid becomes denser as a_* increases, since the ISCO radius changes faster with increasing a_* . The spacing is chosen as a balance between sufficient resolution during interpolation and a reasonable FITS file size. The range of a_* is from 0.71 to 0.9982, since our focus is on rapidly rotating BHs. The range of $\tilde{\gamma}$ is obtained by imposing that our metric describes a black hole with an event horizon, namely the equation $\Delta_r = 0$ has at least a real positive solution. Such a requirement gives an upper bound on $\tilde{\gamma}$, say $\tilde{\gamma} \leq \tilde{\gamma}_{\text{crit}}$. The lower bound is simply zero, following Eq. 9 and since all quantities therein are greater than or equal to zero. The Kerr solution is recovered at $\tilde{\gamma} = 0$. The 36×30 grid for a_* and $\tilde{\gamma}$ is shown in Fig. 2.

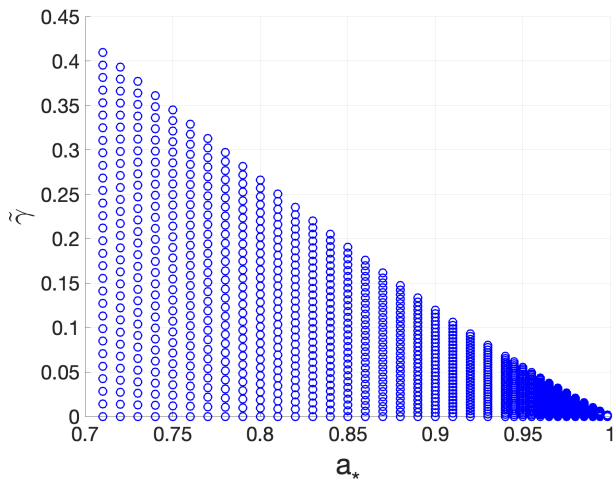


FIG. 2. The grid of values, represented by blue circles, of spin a_* and deformation parameter $\tilde{\gamma}$ for which the transfer functions are calculated and stored in the FITS table. Note that the grid spacings are non-uniform in both a_* and $\tilde{\gamma}$.

For each grid point (i.e., for each a_* , $\tilde{\gamma}$, and i), the accretion disk is discretized in the r_e and the g^* dimension,

with 100 and 40 values, respectively.³ The r_e dimension ranges from the ISCO to $1000M$, and is non-uniform, with higher density near the ISCO. The g^* dimension is equally spaced between ϵ and $1 - \epsilon$, where $\epsilon = 10^{-3}$ (and not 0 and 1 since the transfer function diverges at those values). A fourth order Runge-Kutta ray-tracing scheme, described in [19, 20], traces the photons backwards in time from the telescope screen (placed at asymptotically large distance from the BH) to the disk. Due to the highly curved spacetime near the BH, the landing location of the photon on the disk is not known a priori. An adaptive algorithm is used to fine-tune the initial position of the photon on the telescope screen so that the photon, when ray-traced backwards, lands at the desired r_e . For each such “central” photon, the code calculates the redshift, emission angle, etc. needed for calculation of the transfer function using Eq. 13. Four additional photons are fired for each central photon to calculate the Jacobian in Eq. 13. The initial positions of the additional photons on the telescope screen are chosen to ensure that the resultant Jacobian is convergent. For each r_e , about 100 central photons are computed, which are then interpolated to get the transfer function and the emission angle on the 40 equally spaced values of g^* , which is stored in the FITS file.

IV. DATA ANALYSIS

Having developed the model to calculate reflection spectra for the BH in Eq. 2, we used this model to analyze data from an X-ray binary to constrain the free parameter $\tilde{\gamma}$. In this section, we describe the X-ray source, the observation we used to analyze this source, and the data analysis.

A. Review

GRS 1915+105 (also known as V1487 Aquilae) is a low mass X-binary at a distance of 8.6 kiloparsecs [42]. The mass of the BH in GRS 1915+105 is $\sim 12.4M_\odot$, making it one of the most massive stellar BHs detected in the Milky Way galaxy. It has been a persistent source of X-rays since 1992. It has been extensively analyzed with the RELXILL_NK suite of models, with two observations, one from the *NuSTAR* telescope and the other from the *Suzaku* telescope. In [32], we used RELXILL_NK to analyze the 2012 *NuSTAR* observation. In [33], we analyzed the 2007 *Suzaku* observation. The former observation proved difficult to fit and gave inconsistent values of the deformation parameter analyzed there. The *Suzaku* observation on the other hand required fewer models for a

³Because of the way the transfer function is defined in Eq. 13, it goes to zero when the redshift is maximum or minimum, resulting in two branches of transfer function between $g^* = 0$ and $g^* = 1$.

good fit, and gave consistent best-fit values for the parameters. A difference in the state of the source was also inferred from the observations. The *NuSTAR* observation required a thermal component, suggesting a hotter disk during the observation. The *Suzaku* observation, on the other hand, required no thermal component, suggesting a colder disk during the observation. Since the RELXILL_NK model, which based on XILLVER, assumes a cold disk, the fits with the *Suzaku* observation were deemed more trustworthy.

In [33], the *Suzaku* observation was also analyzed with different versions of RELXILL_NK and different deformation parameters. A qualitative picture emerged thus: the base RELXILL_NK model provides a good fit to the observation, the emissivity profile follows the broken power law, shown in Eq. 11. The emissivity index in the inner parts of the disk is quite large and in the outer parts it is quite small (Such an emissivity profile could be a result of a ring-like corona above the accretion disk [40, 43]), the BH spin is very high (~ 0.99), and the inclination is $\sim 60 - 70$ degrees. Different deformation parameters have been tested with this observation [33, 44]. In all cases, the Kerr limit was covered with high confidence, making the BH consistent with a Kerr BH. Recently, this observation was also analyzed with a thick-disk version of RELXILL_NK [45] (typical models assume an infinitesimally thin disk, this assumption was relaxed in this study). The thick disk RELXILL_NK model provides only a marginally better fit than the base RELXILL_NK model, with no significant difference in the best-fit values of the model parameters.

B. Observations and data reduction

The *Suzaku* observation we will analyze was made on May 7, 2007 for 117 kiloseconds (Obs ID 402071010). Among the four XIS units on board, two were turned off to preserve telemetry and a third unit was running in the timing mode. Therefore we have data from XIS1 only. Additionally, we have data from the HXD/PIN instrument on board.

The details of data reduction for this observation have been given in [32]. We only mention some highlights of the reduced data here, and refer the reader to that reference for further details. The data was grouped to have a minimum of 25 photons per bin. For XIS1, a net exposure time of 28.94 ks in the 3×3 editing mode was achieved. The energy band for data analysis was finalized as 2.3 – 10 keV. The lower bound is due to a lack of sufficient photons below 2.3 keV, and the upper bound is chosen in order to avoid calibration issues near the Si K edge. For the HXD/PIN data, a net exposure time of 53.00 ks was achieved in the 12.0–55.0 keV energy band (the choice of the energy range follows [46]). XSPEC 12.10.1f was used to analyze the data.

C. Modelling and results

Since this observation has been analyzed before with RELXILL_NK, it was natural to begin with the best-fit model combination found previously as a first guess. We thus fit the observation with the following model:

MODEL: TBABS*RELXILL_NK.

Here TBABS accounts for galactic absorption [47]. The galactic column density parameter is kept free during the fitting. The power-law and the reflection components are modeled with RELXILL_NK. The inner edge of the disk is assumed to be at the innermost stable circular orbit, a standard assumption valid in particular for this observation since the Eddington scaled accretion luminosity was 20% during the observation [46, 48, 49], and the outer edge at $400M$ (the fit is not particularly sensitive to the outer radius and therefore we leave it at its default value).

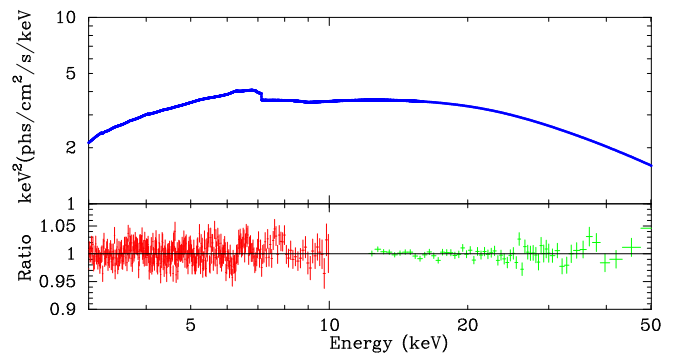


FIG. 3. Top: The spectral model presented in Tab. II. Bottom: Data to model ratio for the spectral fit shown in the top panel. The XIS1 data is in magenta, the HXD/PIN data in blue. See the text for more details.

The best-fit model and the ratio of the data to the model is shown in Fig. 3, in the top and the bottom panels respectively. Note that there are no significant features in the ratio plot, suggesting that the model fits the data well. Tab. II shows the best-fit parameter values and the χ^2 measure of the best-fit. Since the reduced χ^2 is close to 1, the best-fit model provides a good statistical fit to data. We can thus conclude that the model provides a satisfactory fit to the data.

V. DISCUSSION

We now discuss the results of the data analysis presented above. We can compare the best-fit parameter values obtained here with their values in other analyses. Among the BH neighborhood parameters, the emissivity profile, for example, follows previous results, with q_{in} pegged at a large value, and a nearly zero value of q_{out} , with the break occurring near $6M$. Such an emissivity profile is expected for a ring-like corona above the ac-

Model	Best-fit
TBABS	
$N_H/10^{22} \text{ cm}^{-2}$	$8.84^{+0.06}_{-0.04}$
RELXILL_NK	
q_{in}	$9.77^{+(P)}_{-0.21}$
q_{out}	$0.0^{+0.3}$
$r_{\text{br}} [M]$	$6.41^{+0.19}_{-0.60}$
a_*	$0.972^{+0.022}_{-0.019}$
i [deg]	$73.8^{+0.7}_{-0.4}$
Γ	$2.39^{+0.05}_{-0.03}$
$\log \xi$	$2.72^{+0.03}_{-0.02}$
A_{Fe}	$0.53^{+0.06}_{-(P)}$
E_{cut} [keV]	122^{+13}_{-6}
R_f	$0.79^{+0.05}_{-0.04}$
$\tilde{\gamma}$	$0.024^{+0.023}_{-(P)}$
χ^2/dof	$2301.03/2222$ $= 1.03557$

TABLE II. Summary of the best-fit values for the best-fit spectral model. The reported uncertainties correspond to the 90% confidence level for one relevant parameter. For q_{out} there is no lower uncertainty because the best-fit value is stuck at the lower boundary. (P) indicates that the 90% confidence level reaches one of the boundaries of the parameter: the upper boundary of q_{in} is 10, the lower boundary of A_{Fe} is 0.5, and the lower boundary of $\tilde{\gamma}$ is 0.

cretion disk [40, 43]. The spin and inclination are high, the iron abundance is below solar, and the cut off energy is quite low, all of which is consistent with previous results. Of course, the parameter of primary interest in this analysis is the deformation parameter $\tilde{\gamma}$. We find that

$$\tilde{\gamma} \lesssim 0.047, \quad (17)$$

at 90% confidence. This can be directly compared with the results in [6]. There, the authors, using bounds on the mass of M87* obtained by the EHT collaboration [50], provide the following constraint: $\tilde{\gamma} \lesssim 2$, which is significantly weaker than the constraints obtained in the present work. Future observations, of Sgr A*, by EHT are expected to improve the constraints to be: $\tilde{\gamma} \lesssim 0.5$, which is still an order of magnitude weaker than those in Eq. 17.

The difference between our constraint and those from black hole imaging is even more remarkable in terms of γ , which is the real physical parameter for the theory,

because GRS 1915+105 is a stellar-mass black hole while Sgr A* and M87* are supermassive black holes of, respectively, some million and some billion Solar masses. Our constraint is

$$\gamma = \frac{\tilde{\gamma} M^2}{M_{\text{Pl}}^2} \lesssim 6 \cdot 10^{76}. \quad (18)$$

The constraint $\tilde{\gamma} \lesssim 0.5$ from future observations of Sgr A* corresponds instead to $\gamma \lesssim 7 \cdot 10^{88}$.

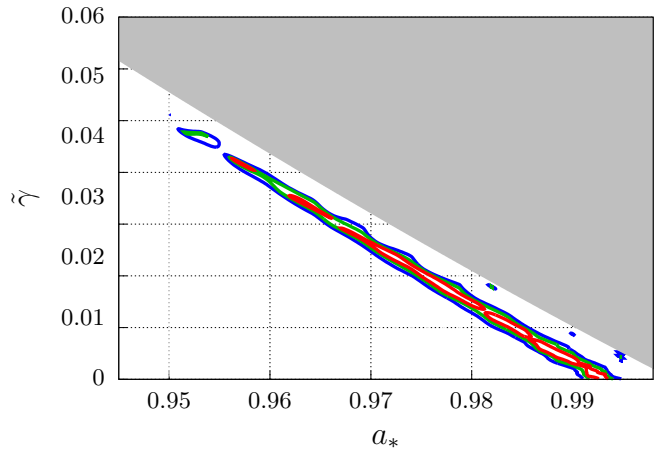


FIG. 4. The contour plot of spin a_* vs. $\tilde{\gamma}$, illustrating the degeneracy between the two parameters. The red, green and blue lines show the 68%, 90%, and 99% confidence level boundaries respectively. The Kerr solution is recovered at $\tilde{\gamma} = 0$. The gray region is ignored in our analysis because in such a region the spacetime has no horizon ($\tilde{\gamma} > \tilde{\gamma}_{\text{crit}}$, see Section III C). See the text for more details.

The results presented above should be seen in the proper context. A crucial source of error in our measurement of $\tilde{\gamma}$ is systematic uncertainty. The RELXILL_NK model makes a series of assumptions about the disk and the corona. Whether these assumption are valid depends on the particular source and the particular observation, and is a matter of debate. Even within the model, inter-parameter degeneracies may result in larger uncertainties. To illustrate, since spin and deformation parameter are generally degenerate, we show a contour plot of a_* vs. $\tilde{\gamma}$ in Fig. 4. The red, blue and green curves are for 68%, 90% and 99% confidence levels, respectively. The degeneracy between spin and $\tilde{\gamma}$ is evident here.

Acknowledgments – This work was supported by the Innovation Program of the Shanghai Municipal Education Commission, Grant No. 2019-01-07-00-07-E00035, and the National Natural Science Foundation of China (NSFC), Grant No. 11973019. A.B.A. acknowledges the support from the Shanghai Government Scholarship (SGS). S.N. acknowledges support from the Alexander von Humboldt Foundation.

- [1] C. M. Will, *Living Rev. Rel.* **17**, 4 (2014), [arXiv:1403.7377 \[gr-qc\]](#).
- [2] C. Bambi, *Rev. Mod. Phys.* **89**, 025001 (2017), [arXiv:1509.03884 \[gr-qc\]](#).
- [3] B. Abbott *et al.* (LIGO Scientific, Virgo), *Phys. Rev. D* **100**, 104036 (2019), [arXiv:1903.04467 \[gr-qc\]](#).
- [4] Z. Carson and K. Yagi, *Class. Quant. Grav.* **37**, 02LT01 (2020), [arXiv:1905.13155 \[gr-qc\]](#).
- [5] F. Vincent, M. Wielgus, M. Abramowicz, E.ourgoulhon, J.-P. Lasota, T. Paumard, and G. Perrin, (2020), [arXiv:2002.09226 \[gr-qc\]](#).
- [6] A. Held, R. Gold, and A. Eichhorn, *JCAP* **06**, 029 (2019), [arXiv:1904.07133 \[gr-qc\]](#).
- [7] P. T. Chrusciel, J. Lopes Costa, and M. Heusler, *Living Rev. Rel.* **15**, 7 (2012), [arXiv:1205.6112 \[gr-qc\]](#).
- [8] C. Bambi, A. D. Dolgov, and A. A. Petrov, *JCAP* **09**, 013 (2009), [arXiv:0806.3440 \[astro-ph\]](#).
- [9] B. Carter, *Phys. Rev. Lett.* **26**, 331 (1971).
- [10] D. C. Robinson, *Phys. Rev. Lett.* **34**, 905 (1975).
- [11] A. Cardenas-Avendano, S. Nampalliwar, and N. Yunes, (2019), [arXiv:1912.08062 \[gr-qc\]](#).
- [12] C. Bambi, *JCAP* **03**, 034 (2014), [arXiv:1308.2470 \[gr-qc\]](#).
- [13] C. Li, S.-F. Yan, L. Xue, X. Ren, Y.-F. Cai, D. A. Easson, Y.-F. Yuan, and H. Zhao, (2019), [arXiv:1912.12629 \[astro-ph.CO\]](#).
- [14] C. S. Reynolds, *Space Sci. Rev.* **183**, 277 (2014), [arXiv:1302.3260 \[astro-ph.HE\]](#).
- [15] C. Bambi, A. B. Abdikamalov, D. Ayzenberg, Z. Cao, H. Liu, S. Nampalliwar, A. Tripathi, J. Wang-Ji, and Y. Xu, *Universe* **4**, 79 (2018), [arXiv:1806.02141 \[gr-qc\]](#).
- [16] Y. Mizuno, Z. Younsi, C. M. Fromm, O. Porth, M. De Laurentis, H. Olivares, H. Falcke, M. Kramer, and L. Rezzolla, *Nat. Astron.* **2**, 585 (2018), [arXiv:1804.05812 \[astro-ph.GA\]](#).
- [17] J. García *et al.*, *Astrophys. J.* **782**, 76 (2014), [arXiv:1312.3231 \[astro-ph.HE\]](#).
- [18] T. Dauser *et al.*, *Mon. Not. Roy. Astron. Soc.* **444**, 100 (2014), [arXiv:1408.2347 \[astro-ph.HE\]](#).
- [19] C. Bambi *et al.*, *Astrophys. J.* **842**, 76 (2017), [arXiv:1607.00596 \[gr-qc\]](#).
- [20] A. B. Abdikamalov, D. Ayzenberg, C. Bambi, T. Dauser, J. A. Garcia, and S. Nampalliwar, *Astrophys. J.* **878**, 91 (2019), [arXiv:1902.09665 \[gr-qc\]](#).
- [21] S. Nampalliwar, S. Xin, S. Srivastava, A. B. Abdikamalov, D. Ayzenberg, C. Bambi, T. Dauser, J. A. Garcia, and A. Tripathi, (2019), [arXiv:1903.12119 \[gr-qc\]](#).
- [22] H. Liu, A. B. Abdikamalov, D. Ayzenberg, C. Bambi, T. Dauser, J. A. Garcia, and S. Nampalliwar, *Phys. Rev. D* **99**, 123007 (2019), [arXiv:1904.08027 \[gr-qc\]](#).
- [23] B. Zhou, A. Tripathi, A. B. Abdikamalov, D. Ayzenberg, C. Bambi, S. Nampalliwar, and M. Zhou, (2019), [arXiv:1908.05177 \[gr-qc\]](#).
- [24] Z. Cao, S. Nampalliwar, C. Bambi, T. Dauser, and J. A. Garcia, *Phys. Rev. Lett.* **120**, 051101 (2018), [arXiv:1709.00219 \[gr-qc\]](#).
- [25] A. Tripathi, S. Nampalliwar, A. B. Abdikamalov, D. Ayzenberg, J. Jiang, and C. Bambi, *Phys. Rev. D* **98**, 023018 (2018), [arXiv:1804.10380 \[gr-qc\]](#).
- [26] Y. Xu, S. Nampalliwar, A. B. Abdikamalov, D. Ayzenberg, C. Bambi, T. Dauser, J. A. Garcia, and J. Jiang, *Astrophys. J.* **865**, 134 (2018), [arXiv:1807.10243 \[gr-qc\]](#).
- [27] K. Choudhury, S. Nampalliwar, A. B. Abdikamalov, D. Ayzenberg, C. Bambi, T. Dauser, and J. A. Garcia, *Astrophys. J.* **879**, 80 (2019), [arXiv:1809.06669 \[gr-qc\]](#).
- [28] M. Zhou, Z. Cao, A. Abdikamalov, D. Ayzenberg, C. Bambi, L. Modesto, and S. Nampalliwar, *Phys. Rev. D* **98**, 024007 (2018), [arXiv:1803.07849 \[gr-qc\]](#).
- [29] M. Zhou, A. Abdikamalov, D. Ayzenberg, C. Bambi, L. Modesto, S. Nampalliwar, and Y. Xu, *EPL* **125**, 30002 (2019).
- [30] A. Tripathi, S. Nampalliwar, A. B. Abdikamalov, D. Ayzenberg, C. Bambi, T. Dauser, J. A. Garcia, and A. Marinucci, *Astrophys. J.* **875**, 56 (2019), [arXiv:1811.08148 \[gr-qc\]](#).
- [31] A. Tripathi *et al.*, *Astrophys. J.* **874**, 135 (2019), [arXiv:1901.03064 \[gr-qc\]](#).
- [32] Y. Zhang, A. B. Abdikamalov, D. Ayzenberg, C. Bambi, T. Dauser, J. A. Garcia, and S. Nampalliwar, *Astrophys. J.* **875**, 41 (2019), [arXiv:1901.06117 \[gr-qc\]](#).
- [33] Y. Zhang, A. B. Abdikamalov, D. Ayzenberg, C. Bambi, and S. Nampalliwar, *Astrophys. J.* **884**, 147 (2019), [arXiv:1907.03084 \[gr-qc\]](#).
- [34] A. Tripathi, A. B. Abdikamalov, D. Ayzenberg, C. Bambi, and S. Nampalliwar, *Phys. Rev. D* **99**, 083001 (2019), [arXiv:1903.04071 \[gr-qc\]](#).
- [35] “RELXILL_NK,” http://www.tat.physik.uni-tuebingen.de/~nampalliwar/relxill_nk/ ().
- [36] “RELXILL_NK,” http://www.physics.fudan.edu.cn/tps/people/bambi/Site/RELXILL_NK.html ().
- [37] I. D. Novikov and K. S. Thorne, in *Proceedings, Ecole d’Eté de Physique Théorique: Les Astres Occlus: Les Houches, France, August, 1972* (1973) pp. 343–550.
- [38] S. Nampalliwar and C. Bambi, (2018), [arXiv:1810.07041 \[astro-ph.HE\]](#).
- [39] E. Kara, J. M. Miller, C. Reynolds, and L. Dai, *Nature* **535**, 388 (2016), [arXiv:1606.06736 \[astro-ph.HE\]](#).
- [40] D. Wilkins and A. Fabian, *Mon. Not. Roy. Astron. Soc.* **414**, 1269 (2011), [arXiv:1102.0433 \[astro-ph.HE\]](#).
- [41] C. T. Cunningham, *Astrophys. J.* **202**, 788 (1975).
- [42] M. Reid, J. McClintock, J. Steiner, D. Steeghs, R. Remillard, V. Dhawan, and R. Narayan, *Astrophys. J.* **796**, 2 (2014), [arXiv:1409.2453 \[astro-ph.GA\]](#).
- [43] G. Miniutti, A. Fabian, R. Goyder, and A. Lasenby, *Mon. Not. Roy. Astron. Soc.* **344**, L22 (2003), [arXiv:astro-ph/0307163](#).
- [44] J. Zhu, A. B. Abdikamalov, D. Ayzenberg, M. Azreg-Ainou, C. Bambi, M. Jamil, S. Nampalliwar, A. Tripathi, and M. Zhou, (2020), [arXiv:2005.00184 \[gr-qc\]](#).
- [45] A. B. Abdikamalov, D. Ayzenberg, C. Bambi, T. Dauser, J. A. Garcia, S. Nampalliwar, A. Tripathi, and M. Zhou, (2020), [arXiv:2003.09663 \[astro-ph.HE\]](#).
- [46] J. Blum, J. Miller, A. Fabian, M. Miller, J. Homan, M. van der Klis, E. Cackett, and R. Reis, *Astrophys. J.* **706**, 60 (2009), [arXiv:0909.5383 \[astro-ph.HE\]](#).
- [47] J. Wilms, A. Allen, and R. McCray, *Astrophys. J.* **542**, 914 (2000), [arXiv:astro-ph/0008425 \[astro-ph\]](#).
- [48] J. F. Steiner, J. E. McClintock, R. A. Remillard, L. Gou, S. Yamada, and R. Narayan, *Astrophys. J.* **718**, L117 (2010), [arXiv:1006.5729 \[astro-ph.HE\]](#).
- [49] A. K. Kulkarni, R. F. Penna, R. V. Shcherbakov, J. F. Steiner, R. Narayan, A. Sadowski, Y. Zhu, J. E. McClintock, S. W. Davis, and J. C. McKinney, *Mon. Not. Roy.*

Astron. Soc. **414**, 1183 (2011), arXiv:1102.0010 [astro-ph.HE].

[50] K. Akiyama *et al.* (Event Horizon Telescope), *Astrophys. J. Lett.* **875**, L6 (2019), arXiv:1906.11243 [astro-ph.GA].